

Hypersonic studies and refractive indices of CsTiOAsO₄ and KTiOAsO₄ single crystals

C.-S. Tu and Y.-L. Yeh

Department of Physics, Fu-Jen University, Taipei, Taiwan, Republic of China

V. H. Schmidt and R.-M. Chien

Department of Physics, Montana State University, Bozeman, Montana 59717

R. S. Katiyar and Ruqian Guo

Department of Physics, University of Puerto Rico, Rio Piedras, Puerto Rico 00931

Ruyan Guo and A. S. Bhalla

Materials Research Laboratory, The Pennsylvania State University, University Park, Pennsylvania 16802

(Received 7 February 1997; revised manuscript received 6 May 1997)

The longitudinal Brillouin backscattering spectra along the [001] phonon direction have been measured as a function of temperature (24–896 °C) for both CsTiOAsO₄ (CTA) and KTiOAsO₄ (KTA). As the temperature approaches the ferroelectric transition temperature T_c , the acoustic phonon frequencies of both CTA and KTA show a strong softening (which reaches a minimum at $T_c \sim 688$ °C for CTA). For both CTA and KTA, a broad damping peak was observed and can be attributed to the dynamic order-parameter fluctuations. This anomaly implies that an $\eta^2\mu$ -type coupling is the dominant mechanism for the acoustic soft modes in CTA and KTA. Here η is the order parameter and μ is the strain. The refractive indices (n_x, n_y, n_z) and Cauchy's equations were obtained as a function of wavelength (0.4–1.7 μm) for KTA. The phase matching angles (θ, ϕ) of second harmonic generation for the fundamental wavelengths of 1.064 (type I) and 1.32 (types I and II) were also calculated. [S0163-1829(97)03437-1]

I. INTRODUCTION

Cesium titanyl arsenate (CsTiOAsO₄) and potassium titanyl arsenate (KTiOAsO₄) belong to the family of nonlinear optical crystals with the general formula $M^{1+}\text{TiOX}^{5+}\text{O}_4$, where $M = \{\text{K, Rb, Tl, Cs}\}$ and $X = \{\text{P, As}\}$.^{1–6} The high damage threshold and broad angular acceptance have made such crystals attractive materials for frequency doubling of Nd-based lasers at $\lambda = 1.064$ and 1.32 μm , and for optical parametric oscillators (OPO). In addition, the ion exchange properties also make them one of the best candidates for waveguide applications. Potassium titanyl phosphate, KTiOPO₄ (KTP), is the most well known among such materials and has been used successfully in different applications.^{1–6} However, the orthophosphate absorption at ~ 4.3 and ~ 3.5 μm in KTP severely limits the oscillator output power. In contrast, both CTA and KTA have a broad infrared transparency (~ 0.35 – 5.3 μm) and exhibits no overtone absorption between 3 and 5 μm . This makes CTA and KTA crystals potential candidates for nonlinear optical applications.

At room temperature, both CTA and KTA have the same orthorhombic structure with noncentrosymmetric point group $C_{2v}(mm2)$ and space group $Pna2$ ($Z=8$). The crystal framework is a three-dimensional structure made from corner-linked TiO₆ octahedra and AsO₄ tetrahedra. Four oxygen ions of the TiO₆ belong to AsO₄ tetrahedral groups which link the TiO₆ groups. In our earlier Raman results,^{1–2} both CTA and KTA display a slightly softening phenomenon on several selected longitudinal (LO) and transverse (TO) vibrational modes. A transition to a higher symmetry struc-

ture (paraelectric phase) taking place at T_c (~ 680 °C for CTA and ~ 880 °C for KTA) was evidenced by the disappearance of the LO $\nu_1(A_{1g})$ stretching mode of the TiO₆ group. In KTA, with careful study of the low frequency region a transverse optical mode with frequency of 42 cm^{-1} at room temperature, belonging to A_1 symmetry, was found to decrease in frequency and increase in its half width exponentially, as the temperature of the sample was raised. We, however, could not follow its behavior above 800 °C due to the reduction in its peak intensity and the presence of another strong lattice mode in this region. There is no typical soft-mode found for both crystals from the Raman spectra for the low-frequency mode as T_c was approached. This motivated us to carry out Brillouin scattering measurements to look for softening in the acoustic mode.

For nonlinear optical materials such as KTP-type crystals, it is always possible to have the fundamental radiation stay in phase with that generated from the second harmonic. In other words, the phase velocity is the same for both the second harmonic and the fundamental waves. Thus, if $n_1(\theta, \phi, \omega)$ and $n_2(\theta, \phi, \omega)$ are the two refractive indices associated with a particular frequency ω and propagation direction (θ, ϕ) , type-I phase matching occurs when $n_1(\theta, \phi, 2\omega) = n_2(\theta, \phi, \omega)$ and type-II phase matching occurs if $n_1(\theta, \phi, 2\omega) = \frac{1}{2}[n_1(\theta, \phi, \omega) + n_2(\theta, \phi, \omega)]$. Here, θ and ϕ are polar coordinates referring to the z axis and the x axis in the x - y plane, respectively.

We report here both the temperature-dependent acoustic phonon spectra (frequency shift, half-width, and susceptibility) and wavelength-dependent refractive indices. The

Cauchy's equations [$n(\lambda) = A + B/\lambda^2 + C/\lambda^4$] of n_x , n_y , and n_z are obtained for KTA. In particular, direct evidence of the acoustic phonon soft modes in both CTA and KTA are presented.

II. EXPERIMENTAL PROCEDURE

CsTiOAsO₄ and KTiOAsO₄ single crystals were grown using the tungstate flux method. The crystals were oriented by x-ray diffraction and were cut into rectangular shapes having (100), (010), and (001) faces. The dimensions of crystals are $4.2 \times 2.9 \times 2.1$ and $3.6 \times 3.6 \times 1.9$ mm³ for CTA and KTA, respectively. The surfaces for measurements were polished to be optically smooth. In our experiments the Brillouin spectra were obtained from the backscattering geometry with scattering configuration $Z(XU)\bar{Z}$. Here, U means that the collection was not polarization discriminated. The sample was illuminated along the [001] (z -axis) phonon direction, by a Lexel Model 95-2 argon laser with $\lambda = 514.5$ nm, so the longitudinal phonons with wave vector along [001] were studied. Scattered light was analyzed by a Burleigh five-pass Fabry-Pérot interferometer. To acquire more accurate data of frequency shift and half-width, the Brillouin doublets were adjusted to appear in the second order with respect to the Rayleigh line. In other words, the free spectral range (FSR) is less than the Brillouin shift of the LA[001] phonon. The laser power incident on the samples was kept less than 100 mW. A new calibrated R -type thermocouple was used to read sample temperature. The samples were heated from room temperature by steps and the data were collected automatically. Results were found to be reproducible.

In order to determine the position and half-width of the Brillouin component, the damped harmonic oscillator model with the spectral response function⁷

$$S(\omega) = \frac{\chi_0 \Gamma \omega \omega_0^2}{(\omega^2 - \omega_0^2)^2 + \Gamma^2 \omega^2} \frac{1}{1 - e^{-\hbar \omega / \kappa T}} \quad (1)$$

was used, where ω_0 and Γ correspond to the phonon frequency and half width, respectively. χ_0 is the susceptibility constant (in arbitrary units). κ is Boltzmann's constant and T is absolute temperature. In our experiments, the free spectral ranges are 24.11 GHz (for CTA) and 26.83 GHz (for KTA) determined by measuring the LA phonon shift of fused quartz.

For measurements of refractive indices, a J. A. Woollam Co. Model VB-200 variable angle spectroscopy ellipsometer was used with WVASE32™ analyzing software. A xenon gas lamp was used for the light source. The refractive indices were determined by measuring the change of polarization between incident and reflected beams. The KTA sample was measured from 0.4 to 1.7 μm with intervals of 0.01 μm . However, we could not obtain good refractive spectra from the CTA crystal due to its small size.

III. RESULTS AND DISCUSSION

A. Brillouin spectra and related calculations

Actual LA[001] phonon spectra of both anti-Stokes and Stokes Brillouin components are shown in Figs. 1(a) and 1(b) for CTA and KTA, respectively. The solid lines are fits

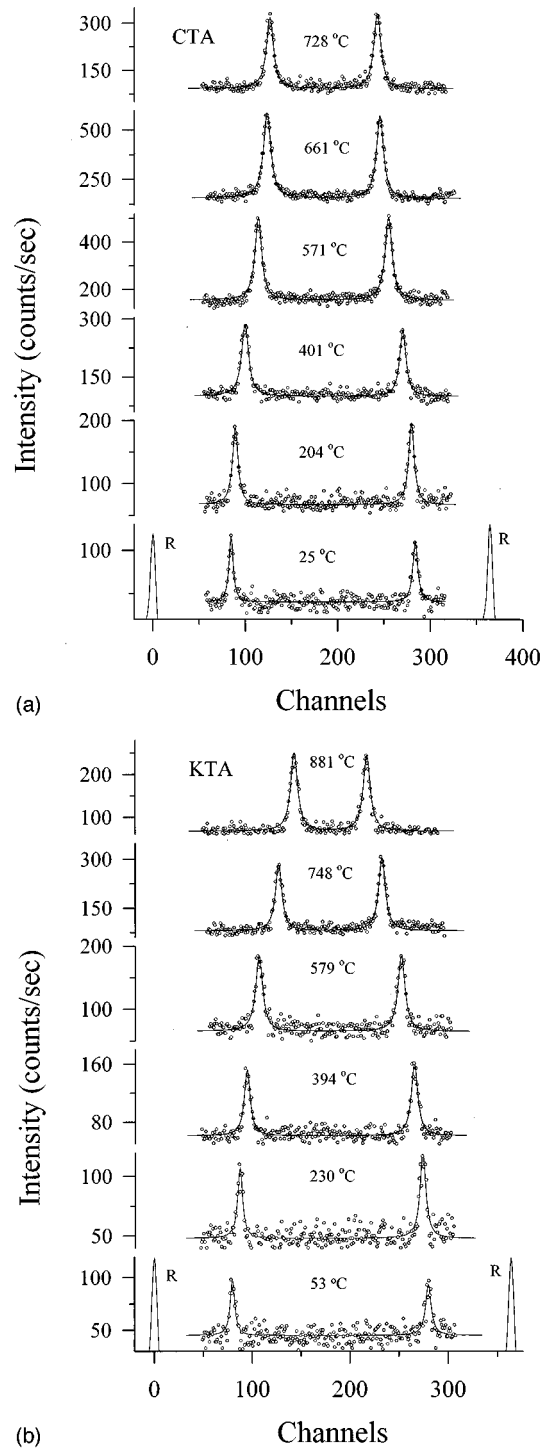


FIG. 1. Anti-Stokes and Stokes components of the LA[001] Brillouin spectra for (a) CTA and (b) KTA. The frequency intervals (FSR) between the two Rayleigh (R) peaks are 24.11 and 26.83 GHz for CTA and KTA, respectively.

of Eq. (1), from which the frequency shift, half-width Γ , and susceptibility constant χ_0 were obtained. As evidenced in the spectra, the frequency shift temperature dependences of both crystals indicate a strong acoustic coupling effect (negative contribution) with increasing temperature.

In order to estimate the coupling effect, we calculated the bare (uncoupled) phonon frequency $\omega_a(T)$, by fitting the measured frequency shifts at low-temperature region (in the

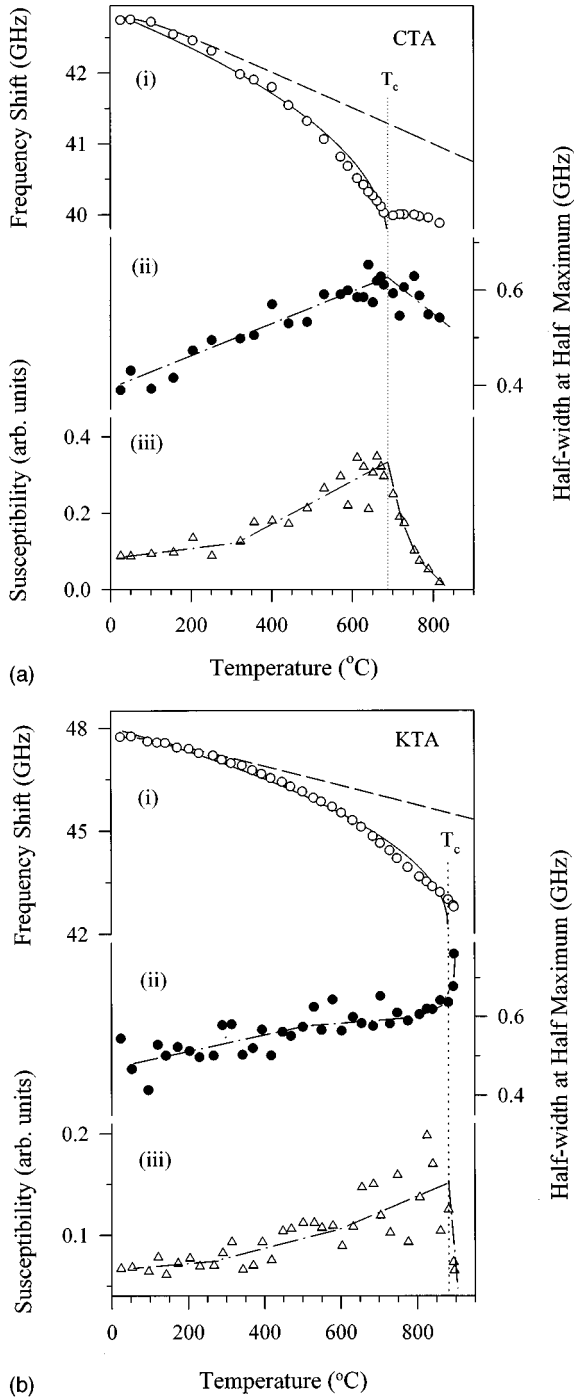


FIG. 2. Temperature dependences of different characteristics: (i) Brillouin shift (open circle), (ii) half-width (solid circle), and (iii) susceptibility constant (triangle), for (a) CTA and (b) KTA. The dotted lines indicate the ferroelectric phase transition temperatures $T_c \sim 688$ and ~ 880 °C for CTA and KTA, respectively. The dot-dashed lines are guides to the eye.

uncoupled region). The bare phonon frequency is defined as the phonon frequency far from the phase transition temperature. The temperature dependence of $\omega_a(T)$ can be described by the Debye anharmonic approximation⁸

$$\omega_a(T) = \omega_a(0) \left[1 - A \Theta F\left(\frac{\Theta}{T}\right) \right], \quad (2)$$

TABLE I. Parameters from the fits of Eq. (2) to high-temperature measured values of frequency shift.

	$\omega_a(T=0)$ (GHz)	A (K^{-1})	Θ (K)
CTA	42.78	6×10^{-5}	300
KTA	47.75	6×10^{-5}	300

where Θ is the Debye temperature, A represents the amount of anharmonicity, and $F(\Theta/T)$ is the Debye function for internal energy⁹

$$F\left(\frac{\Theta}{T}\right) = \frac{3}{(\Theta/T)^4} \int_0^{\Theta/T} \frac{u^3}{e^u - 1} du, \quad (3)$$

as tabulated, for example, by Abramowitz and Stegun.¹⁰

The temperature dependences of the frequency shift, half-width, and susceptibility constant for CTA and KTA are shown in Figs. 2(a) and 2(b), respectively. The dashed lines in the frequency shifts are the calculations of Eq. (2) with the parameters of Table I. Here we assume that temperatures near room temperature are far away from the coupled region since the ferroelectric phase transitions occur around 680 and 880 °C for CTA and KTA, respectively. As shown in Figs. 2(a) and 2(b), the measured phonon frequencies depart from the bare frequencies near 200 °C (in CTA) and 300 °C (in KTA). In other words, the acoustic soft modes begin to set in above 200 and 300 °C in CTA and KTA, respectively. For a typical second-order FE phase transition, the transition temperature occurs where the frequency shift curve is steepest. In CTA, the acoustic phonon frequency has an abrupt change with increasing temperature and reaches a minimum at ~ 688 °C. Thus, the FE transition temperature T_c in CTA is ~ 688 °C. This value compares well with those previous reported; Loiacono *et al.*, 671 ± 5 °C and Marnier *et al.*, 679 °C.^{3,6} As temperature increases, the phonon shift of KTA also shows a rapid softening but with a residual value at $T_c \sim 880$ °C. This behavior implies that the structural transition instability in KTA must be associated with some other excitation, perhaps the central mode.

The solid lines in Figs. 2(a) and 2(b) are the fits using the equation $\omega = a(T_c - T)^{1/2} + b$ with the parameters listed in Table II. We note that a zone-center ($q_0 = 0$) acoustic soft mode in the reduced Brillouin zone of the reciprocal sublattice always has a zero frequency as $T \rightarrow T_c$, i.e., $b = 0$.¹¹ Therefore, the nonzero minimum of frequency shift at T_c implies that the ferroelectric phase transition in CTA must be associated with the more complicated non-zone-center mode(s) ($q_0 \neq 0$).

The phonon dampings [shown in Figs. 2(a) and 2(b)] of both CTA and KTA exhibit a gradual growth from room temperature up to near T_c . Such a slowly rising damping anomaly is associated with the dynamic order parameter

TABLE II. Parameters from the fits of equation $\omega = a(T_c - T)^{1/2} + b$ to measured values of frequency shift.

	a (GHz/°C ^{1/2})	b (GHz)	T_c (°C)
CTA	0.125	39.6	688
KTA	0.194	42.2	880

TABLE III. Refractive indices n_z , longitudinal sound velocities V_{LA} , and elastic constants $C_{33}^E + (e_{33}^2/\epsilon_{33}^s)$ of CTA and KTA at room temperature from backscattering.

	n_z (514.5 nm)	V_{LA} (m/sec)	$C_{33}^E + (e_{33}^2/\epsilon_{33}^s)$ (10^{11} N/m 2)
CTA	1.995	5513	1.37
KTA	1.932	6357	1.41

fluctuations. The dot-dashed curves in Figs. 2(a) and 2(b) are guides to the eye. As one knows, the dynamic order parameter fluctuations for longitudinal acoustic phonons are characteristic of an $\eta^2\mu$ -type electrostrictive coupling, squared in order parameter and linear in strain.¹²

As shown in Figs. 2(a) and 2(b), a broad growth from room temperature to T_c was also observed in the temperature dependences of susceptibility constant in both CTA and KTA crystals. A static uniform susceptibility of Curie-Weiss form, $\chi_0 = \beta/|T_c - T|$,¹¹ cannot explain this strong broad anomaly in susceptibility. This indicates that dynamic fluctuations become the governing mechanism for the structural instabilities of CTA and KTA as T approaches T_c .

Brillouin scattering is a powerful tool to determine the related acoustic parameters such as elastic constants. The associated theories and calculations of connected parameters can be found in Ref. 13. At room temperature, the densities are $\sim 4.51 \times 10^3$ and $\sim 3.48 \times 10^3$ kg/m 3 for CTA and KTA, respectively. In our experiment, the measured phonon is along the [001] direction ($\vec{q}/[001]$). By solving the secular equation (3) of Ref. 13, one obtains

$$\rho V_{LA}^2 = \rho \left(\frac{\lambda_0 \Delta \nu_{LA}}{2n \sin(\theta/2)} \right)^2 = C_{33}^E + \frac{e_{33}^2}{\epsilon_{33}^s}, \quad (4)$$

where λ_0 is the wavelength of the incident light in vacuum, θ is the scattering angle in the crystal, $\Delta \nu_{LA}$ is the longitudinal phonon frequency shift, e_{ij} is the piezoelectric stress constant, and ϵ_{ij}^s is the permittivity at constant strain. The related calculated values from the Brillouin spectra for both CTA and KTA are listed in Table III. One can expect that the smaller sound velocity and elastic constant in CTA are mainly due to the heavier cesium atomic mass. Here the refractive index (n_z) of CTA was taken from Ref. 5.

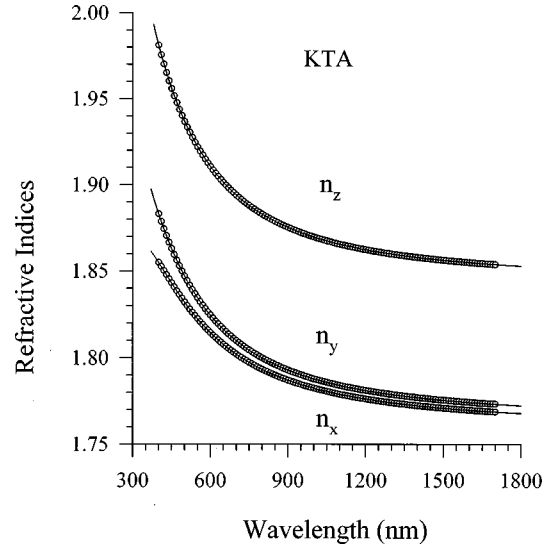


FIG. 3. Refractive indices (n_x, n_y, n_z) of KTA. Solid lines are fits to the Cauchy's equations with parameters given in Eq. (5).

B. Refractive indices and phase matching angles of KTA

Figure 3 shows the refractive indices of n_x , n_y , and n_z measured at room temperature. The solid lines are the fits of Cauchy's equations with parameters

$$\begin{aligned} n_z(\lambda) &= 1.8453 + \frac{0.02486}{\lambda^2} - \frac{0.0005}{\lambda^4}, \\ n_y(\lambda) &= 1.7654 + \frac{0.02318}{\lambda^2} - \frac{0.0007}{\lambda^4}, \\ n_x(\lambda) &= 1.7612 + \frac{0.02248}{\lambda^2} - \frac{0.0012}{\lambda^4}. \end{aligned} \quad (5)$$

The unit of wavelength (λ) in Eq. (5) is μm . We summarize the refractive indices of four wavelengths in Table IV with the earlier results obtained by measuring the critical angle of refraction.¹⁴ Our refractive indices and birefringences of KTA agree reasonably well with the results of Cheng *et al.*¹⁴ As shown in Table IV, the intrinsic optical birefringence of KTA decreases with increasing wavelength. The birefringence ($n_z - n_x = 0.0868$ at $1.064 \mu\text{m}$) of KTA is smaller than for KTP ($n_z - n_x = 0.0921$ at $1.064 \mu\text{m}$).¹⁵ This reduction of birefringence makes KTA an ideal material for

TABLE IV. Refractive indices and birefringences ($n_z - n_x$) of KTA for four wavelengths.

λ (μm)	n_x	n_y	n_z	$n_z - n_x$	
0.633	1.8098	1.8189	1.9042	0.0944	present work
	1.8083	1.8142	1.9048	0.0965	Ref. 14
0.66	1.8065	1.8149	1.8997	0.0932	present work
	1.8042	1.8104	1.8997	0.0955	Ref. 14
1.064	1.7801	1.7853	1.8669	0.0868	present work
	1.7812	1.7866	1.8675	0.0863	Ref. 14
1.32	1.7737	1.7785	1.8594	0.0857	present work
	1.7751	1.7798	1.8589	0.0838	Ref. 14

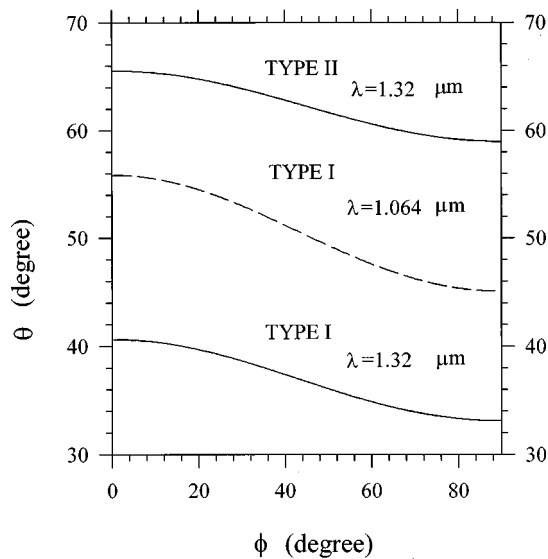


FIG. 4. SHG phase matching angles (θ, ϕ) of types I and II for KTA, plotted on the first quadrant. The solid and dashed lines correspond to the fundamental wavelengths 1.32 and 1.064 μm , respectively.

frequency doubling at higher fundamental wavelengths such as 1.32 μm for the Nd:YAG laser line.

The accuracy of the refractive indices can be checked by comparing the calculated phase matching angles (θ, ϕ) with the experimental data. For a biaxial crystal, the derivation of phase matching angles for second harmonic generation can be found in Ref. 16. Figure 4 shows the propagation directions for phase matching frequency doubling for $\lambda = 1.32 \mu\text{m}$ (types I and II) and $\lambda = 1.064 \mu\text{m}$ (type I). Nevertheless, phase matching propagation for type-II frequency doubling at 1.064 μm is not allowed. In the y - z plane ($\phi = 90^\circ$), our calculated phase matching angle θ_{pm} is 59° (for type II) which agrees quite well with the earlier experimental result $\theta_{\text{pm}} = 56^\circ$.⁹ Compared with the phase matching curves (for $\lambda = 1.32 \mu\text{m}$) for KTP,¹⁵ KTA has a higher phase matching angle θ for both types I and II while ϕ is fixed. This shift of phase matching angle is believed to be associated with the smaller birefringence in KTA.

IV. CONCLUSIONS

A main feature of the LA[001] acoustic phonon spectra in both CTA and KTA is that a strong temperature-dependent character has been observed in the frequency shift, half-width, and susceptibility. As temperature increases from the ordered phase, the acoustic phonon soft modes begin to embed at ~ 200 and $\sim 300^\circ\text{C}$ in CTA and KTA, respectively. The phonon frequency of CTA reaches a nonzero minimum at $T_c \sim 688^\circ\text{C}$ and this softening anomaly is connected with the non-zone-center mode(s) ($q_0 \neq 0$). However, the phonon frequency of KTA continues to soften even above $T_c \sim 880^\circ\text{C}$ as temperature increases. This residual behavior implies that the structural transition instability (near T_c) in KTA must be associated with some other excitation, perhaps the central mode. From the temperature dependences of phonon half-width, we conclude that dynamic order parameter fluctuations are the dominant mechanism for the slowly rising damping anomalies in both CTA and KTA. A quadratic $\eta^2\mu$ -type electrostrictive coupling, squared in order parameter and linear in strain, is considered to be the main contribution to the acoustic phonon softening in both crystals.

The refractive indices (n_x, n_y, n_z) of KTA single crystal have been measured and show a strong wavelength-dependent character between 0.4 and 1.7 μm . The phase matching angles (θ, ϕ) of second harmonic generation for fundamental wavelengths 1.064 (type I) and 1.32 μm (types I and II) were calculated, respectively. The birefringence of the KTA crystal was found to be too low for type-II phase matching frequency doubling at 1.064 μm .

ACKNOWLEDGMENTS

The authors would like to sincerely thank Bing-Jong Jang for his help with the calculations. This work was supported by Grant No. NSC-86-2112-M-030-002 (R.O.C.), U.S. DOE Grant No. DE-FG02-94ER75764, and NSF Grant No. DMR-9520251.

¹C.-S. Tu, A. R. Guo, Ruiwu Tao, R. S. Katiyar, Ruyan Guo, and A. S. Bhalla, *J. Appl. Phys.* **79**, 3235 (1996).

²A. R. Guo, C. S. Tu, Ruiwu Tao, R. S. Katiyar, Ruyan Guo, and A. S. Bhalla, *Ferroelectr. Lett. Sect.* **21**, 71 (1996).

³G. M. Loiacono, D. N. Loiacono, and R. A. Stolzenberger, *J. Cryst. Growth* **131**, 323 (1993).

⁴G. M. Loiacono, *Appl. Phys. Lett.* **64**, 2457 (1994).

⁵L. T. Cheng, L. K. Cheng, J. D. Bierlein, and F. C. Zumsteg, *Appl. Phys. Lett.* **63**, 2618 (1993).

⁶G. Marnier, B. Boulanger, and B. Menaert, *J. Phys.: Condens. Matter* **1**, 5509 (1989).

⁷J. F. Ryan, R. S. Katiyar, and W. Taylor, *Effet Raman Et Théorie* **C2**, 49 (1971).

⁸C.-S. Tu and V. H. Schmidt, *Phys. Rev. B* **50**, 16 167 (1994).

⁹C. Kittel, *Introduction to Solid State Physics*, 5th ed. (Wiley, New York, 1976), p. 137.

¹⁰*Handbook of Mathematical Functions*, 7th printing, edited by M. Abramowitz and I. A. Stegun (Dover, New York, 1970), p. 998.

¹¹M. E. Lines and A. M. Glass, *Principles and Applications of Ferroelectrics and related Materials* (Oxford University Press, London, 1977).

¹²W. Rehwald, *Adv. Phys.* **22**, 721 (1973).

¹³C.-S. Tu, V. H. Schmidt, and I. G. Siny, *J. Appl. Phys.* **78**, 5665 (1995).

¹⁴L. K. Cheng, L.-T. Cheng, J. D. Bierlein, and F. C. Zumsteg, *Appl. Phys. Lett.* **62**, 346 (1993).

¹⁵Y. F. Tso, C. E. Huang, B. Q. Hu, R. C. Eckardt, Y. X. Fan, R. L. Byer, and R. S. Feigelson, *Appl. Opt.* **26**, 2390 (1987).

¹⁶J. Q. Yao and T. S. Fahlen, *J. Appl. Phys.* **55**, 65 (1984).